Edge Turbulence, Blob Generation, and Interaction with Sheared Flows

D. A. D'Ippolito 1)**, J. Boedo** 2)**, D. P. Lundberg** 3)**, R. Maqueda** 4)**, J. R. Myra** 1)**, D. A. Russell** 1)**, D. P. Stotler** 3) **and S. J. Zweben** 3)

1) Lodestar Research Corporation, Boulder, Colorado, USA
2) University of California San Diego (UCSD), San Diego, California, USA
3) Princeton Plasma Physics Laboratory (PPPL), Princeton, New Jersey, USA
4) Nova Photonics, Princeton, New Jersey, USA

August, 2008

Presented at the 22nd IAEA Fusion Energy Conference
October 13-18, 2008, Geneva, Switzerland
paper IAEA-CN-165/TH/P4-17

DOE/ER/54392-48; ER/54678-3 LRC-08-124

Lodestar Research Corporation
2400 Central Avenue
Boulder, CO 80301

Edge Turbulence, Blob Generation, and Interaction with Sheared Flows*

D. A. D'Ippolito 1), J. Boedo 2), D. P. Lundberg 3), R. Maqueda 4), J. R. Myra 1), D. A. Russell 1), D. P. Stotler 3) and S. J. Zweben 3)

1) Lodestar Research Corporation, Boulder, Colorado, USA
2) University of California San Diego (UCSD), San Diego, California, USA
3) Princeton Plasma Physics Laboratory (PPPL), Princeton, New Jersey, USA
4) Nova Photonics, Princeton, New Jersey, USA

e-mail contact of main author: dippolito@lodestar.com

Abstract. A program of 2D simulations of edge turbulence and blob generation using the Lodestar SOLT code is described. Issues studied include the transport of particles and poloidal momentum in the edge and SOL, the processes by which momentum transport drives sheared poloidal flow layers in the edge plasma, the nonlinear turbulence saturation mechanisms producing the blobs, and the interaction of blob generation with sheared flows. If the sheared flows are sufficiently strong, they can stabilize the underlying instability and saturate the turbulence. If the flows are weak, the saturation occurs by turbulent modification of the density profile (plateau formation or wave-breaking). A new synthetic gas-puff-imaging (GPI) diagnostic in the code has been used to compare the simulations with GPI data for the NSTX experiment. Statistics for the turbulent fluctuations and the blobs are compared between simulations and data. The conditions for obtaining qualitative agreement for one L-mode shot are described.

1. Introduction

There has been a great deal of experimental and theoretical work devoted to the study of convection of coherent objects (blobs and ELMs) in the scrape-off-layer (SOL) of toroidal and linear plasma devices (see the review in [1] and references therein). In tokamaks, SOL convection driven by toroidal curvature appears to be a universal phenomenon that can interrupt the particle flow to the divertor, increase plasma interaction with the first wall, and enhance impurity transport into the core. These effects could cause significant degradation of performance in ITER or in a tokamak fusion reactor. On the other hand, turbulent convection of momentum from the edge plasma to the wall may induce rotation of the core plasma [2 - 4] that can improve the magnetohydrodynamic stability of ITER. The goal of the simulations and experimental comparisons reported here is to identify the important physics issues determining the scaling of the convective transport.

In this paper, we summarize the results of recent simulations using the Lodestar SOLT turbulence code which address a number of related questions: nonlinear saturation mechanisms for edge turbulence, the role of sheared flow in regulating both turbulence and blob generation, the turbulent transport of perpendicular momentum across the last closed surface by both Reynold's stress and blob convection, and the role of sheath and plasma dissipation in all of these processes. Also, we discuss a comparison of the simulations with NSTX gas puff imaging (GPI) data using a new synthetic GPI diagnostic in the code.

2. Simulation Model

Previous work with the SOLT code used a two-region model which coupled two simulation planes (midplane, divertor) to permit variation of the curvature-driven turbulence along the field line due to collisional effects (reduced parallel conductivity) and magnetic geometry effects (X-points and magnetic shear). It was shown that the turbulent flux (and blob velocity) in the SOL increases with collisionality (for fixed geometry) and decreases due to X-point effects (at fixed collisionality) [5]. These result could be understood in terms of the

flow of electrical current in the blob circuit [5, 6], viz. the blob velocity is proportional to the total resistance in the circuit, which is determined by both the parallel and perpendicular plasma resistance ($\propto$ collisionality) and the sheath resistance. Zonal flow was suppressed in these simulations. The next step was to include sheared flow in the binormal ($\hat{\mathbf{e}}_r \times \mathbf{b}$) direction and to investigate the complicated interplay between sheared flow and turbulence, and the effect of this interplay on both particle and momentum flux.

In the present work, the code has been modified to treat flows and momentum transport. We solve a reduced set of equations [3, 7] numerically for the evolution of vorticity, density, temperature and zonal fluid momentum, in the two dimensions orthogonal to the magnetic field in the edge and SOL of a tokamak. To keep the code as streamlined as possible, only a single (midplane) region is employed for the work discussed in this paper, but the physics model is generalized to include drift-wave terms, which provide directionality and drive flows in the edge plasma. Another new feature is a momentum-conserving treatment for the zonally-averaged flows [7]. The input profiles are chosen to model the edge-SOL boundary, with drift-wave physics inside the last closed surface (LCS), sheath dissipation outside the LCS, and uniform curvature. A new synthetic diagnostic has also been added to the SOLT code which calculates the GPI intensity for given density, temperature, and neutral profiles.

3. Perpendicular Momentum Transport

It has been suggested that turbulence transports plasma momentum out of the core region and towards the wall, providing a momentum "source" that can induce net core plasma rotation as well as sheared zonal flows in the edge [2]. Motivated by this idea, preliminary results on turbulent momentum transport were reported at the last IAEA meeting [3]; a more complete analysis [7] has since been carried out for momentum in the binormal direction, perpendicular to both the radial (x) and magnetic field (z) directions.

The 2D simulations show that turbulence in the vicinity of the last closed surface transports plasma momentum away from the core region towards the wall, and hence provides a momentum "source" that can induce net core plasma rotation as well as sheared flows in the edge [3, 7]. The net momentum transferred to the core is influenced by a number of physical effects: dissipation, the competition between momentum transport by Reynolds stress and passive convection by particles, intermittency (the role of blobs carrying momentum), and velocity shear regulation of turbulence.

Some specific results from the simulations: (1) The generation of net flow (as opposed to local bipolar flows) requires momentum loss in the SOL by sheath dissipation. (2) The Reynolds stress contribution $\langle n\rangle\langle v_x v_y\rangle$ is opposed by the passive loss of momentum $\langle nv_x\rangle\langle v_y\rangle$ carried by exiting particles, where $\langle\ldots\rangle$ is an ensemble (y, t) average. The two terms nearly cancel, but the Reynolds term was slightly larger in our simulations. (3) Transport of perpendicular momentum across the LCS is dominated by turbulent (drift-curvature driven) fluxes in a radial region just inside the LCS where blob formation is not yet complete. Thus, in the steady turbulent state, the *blob* transport of momentum is a small effect. This is illustrated in *FIG. 1*, which compares the normalized probability distribution functions (PDFs) of the particle flux (dashed line) and momentum flux (solid line) at the LCS. Note that the left-right

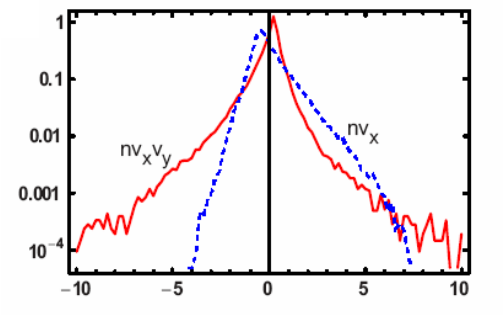

FIG. 1 Probability distribution function (PDF) of particle flux (blue dashed line) and momentum flux (red solid line)

asymmetry (related to the skewness) is much greater for the particle flux than for the momentum flux, confirming that blobs play a reduced role in momentum transport. A related observation is that for steady-state turbulence, the particles transport by larger, more coherent structures than the momentum. However, significant blob-related momentum transport can occur as a transient response, e.g. due to rapid changes in the core-side gradients and/or sheared flows. (4) Another significant result is that the edge momentum source adjusts to match the rate of momentum transfer into the core, keeping the edge velocity shear nearly constant. This result suggests the importance of the sheared flow in regulating the turbulence.

4. Turbulence Saturation and Role of Sheared Flow

A series of simulations was carried out to investigate the physical mechanism responsible for nonlinear saturation of the turbulence. A damping term $(-\nu_{py}\,\bar{p}_y)$ was included in the zonally-averaged momentum equation, and the parameter ν_{py} was varied from 0 to ∞. It was found that there are two regimes (*see FIG. 2*):

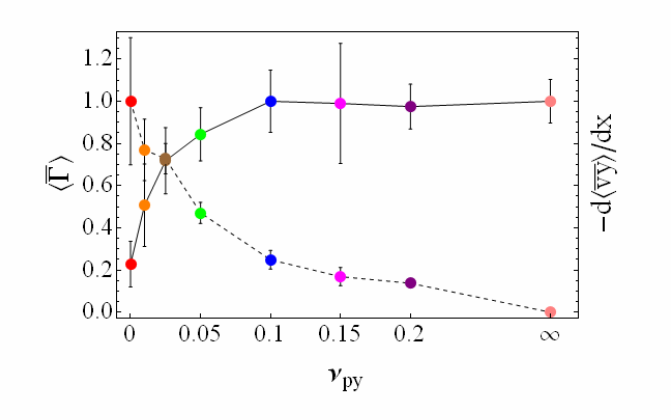

FIG. 2 Plots of sheared flow (dashed line) and radial particle flux (solid line) vs flow dissipation

(a) In the limit $\nu_{py} \to \infty$, the zonal flow is absent, the turbulence saturates at a relatively high level, and it produces convecting objects that look more like radial streamers than blobs. The time-history of the turbulent flux shows *quasi-periodic* oscillations, and it appears to saturate by *wave-breaking*, i.e. the condition $< \nabla \delta n_{rms} / \nabla \bar{n} > \sim 1$ is satisfied near the surface of maximum growth rate. Physically, this condition is satisfied because the large turbulent flux causes density plateau formation outside the LCS, reducing $\nabla \bar{n}$. Note that in Secs. 4 and 5 an overbar denotes a zonal average and <…> denotes a time average.

(b) In the limit $\nu_{py} \to 0$, the zonal flow is strong, the turbulence saturates at a lower level and produces convecting objects that look blob-like. The time-history of the turbulent flux shows *intermittent* bursts, and the turbulence saturates as a result of the stabilizing effect of the *sheared flow*s.

There is a smooth transition from the sheared-flow to the wave-breaking regime as ν_{py} increases. This is shown in *FIG. 2* for both the particle flux $\Gamma =< n v_x >$ and for the sheared flow in the binormal (approximately poloidal) direction, $-d < \bar{v}_y > / dx$. Both quantities are normalized to have peak values of unity. The flux is measured at the "sheath position" (Δr = 4.42 cm), while the sheared flow is measured at Δr = 0. Here, Δr is the radial distance from the nominal LCS (defined at the mid-plane) with $\Delta r > 0$ in the SOL. (In this paper, we use x and Δr interchangeably.) The significance of the region $0 < \Delta r < \Delta r_{sh}$ = 4.42 cm (where field

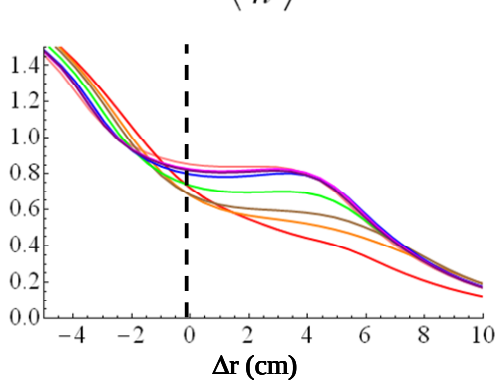

FIG. 3 Plot of average density profile for several values of flow dissipation parameter ν_{py}.

lines are assumed disconnected from the sheath) is discussed in more detail in Sec. 5.

The transition between the two turbulence saturation regimes is also evident in *FIG. 3*, which shows the density profiles $<\bar{n}>(\Delta r)$ for several values of flow damping, and the resulting density plateau formation at large ν_{py}. The colors of the curves correspond to those of the data points in *FIG. 2* and thus label ν_{py}. The vertical dashed line indicates the nominal position of the LCS. Only a small amount of sheared flow damping is needed to produce a large increase in turbulent radial particle flux (*FIG. 2*) and thus develop a significant density plateau in the near SOL (*FIG. 3*). This nonlinear evolution of the density profile saturates the turbulence by reducing the instability drive. As in the two-region model collisionality studies mentioned in Sec. 2, we find that a relevant dissipation parameter (here ν_{py}) plays a key role in determining the transport.

One can estimate analytically the flux saturation levels in the limits of weak and strong sheared flows and the transition point.

In the limit $\nu_{py} \to \infty$ we use the wavebreaking condition, $k_y \tilde{n} = \nabla_x \bar{n}$, combined with the continuity equation, $\gamma \tilde{n} = k_y \tilde{\phi} \nabla_x \bar{n}$, and the definition of particle flux, $\Gamma = <\tilde{n}\tilde{v}_x>$, to get an estimate of the particle flux at saturation, $\Gamma_{sat}(\nu_{py} \to \infty) \sim \gamma \nabla_x \bar{n} / k_y^2$, where $\gamma = c_s (L_n R_c)^{-1/2}$ is the growth rate of the curvature ($\sim 1/R_c$) driven interchange mode. For the most highly damped case in *FIG. 2*, we find that the growth rate is significantly lower than this estimate. If we use the numerically determined growth rate, the wavebreaking estimate for Γ_{sat} agrees with the computed turbulent flux to within a factor of 2.

In the limit $\nu_{py} \to 0$, the condition for sheared flow to stabilize the mode is $\gamma \sim \bar{v}_y' \sim \bar{v}_y / L_v$. Balancing the Reynolds stress term in the vorticity equation with the damping term, we obtain the scaling $\bar{v}_y = (k_x / k_y)^2 (k_y^3 |\tilde{\phi}|^2) / \nu_{py}$. Finally, using the continuity equation and the definition of particle flux, we obtain the following estimate of the saturated particle flux: $\Gamma_{sat} = <\tilde{n}\tilde{v}_x> \sim (k_y / k_x)^2 (\bar{n} \nu_{py} L_v) / (k_y L_n)$. Using the simulation parameters for the case $\nu_{py} = 0.04$ (the "knee" of the curve in *FIG. 2*), we find that this formula gives good agreement with the computed turbulent particle flux.

Thus, for small zonal flow damping our estimate of the saturated turbulent particle flux Γ_{sat} is proportional to ν_{py} and independent of growth rate γ; for large damping, Γ_{sat} is independent of ν_{py} and proportional to γ. These scalings agree with the numerical results shown in *FIG. 2*. Equating the two expressions gives an estimate of ν_{py} at the knee of the curve which marks the transition between the two regimes.

Finally, we mention that NSTX parameters were used for the runs in these figures, similar to those discussed in the next section. However, in the NSTX modeling we set $\nu_{py} \to 0$ so that the full zonal flow dynamics are retained.

5. NSTX Modeling

The simulations described above contain enough physics that it is reasonable to ask whether such a model could reproduce some aspects of experimental edge turbulence data. We have carried out an extensive comparison of the SOLT simulations with the 2D gas-puff-imaging (GPI) data on NSTX, which allows a degree of comparison with theory not previously achieved using 1D time series data from probes.

The idea of the GPI diagnostic is to puff a small amount of neutral gas for diagnostic purposes (helium in the shot analyzed here, but deuterium in most shots) into the SOL plasma and view the resulting visible light emission by a fast camera. The result is a time sequence of 2D (radial-poloidal) images (a "movie"), showing the light emission, $I = n_0 f(n_e, T_e)$, where n_0 is the neutral density of the puff and $f(n_e, T_e)$ is the effective emission rate obtained from a collisional radiative (CR) model of the helium atom [8]. Viewed along the B field line, the emission provides a visualization of the turbulence and blob dynamics normal to **B**. Given knowledge of the radial profile of the injected gas, $n_0(x)$, and and the helium CR model, together with a passive-convection ansatz, the local plasma density and temperature fluctuations can be extracted from the GPI data [9]. Here, we take the opposite approach. A synthetic diagnostic is implemented in the SOLT code using $f(n_e, T_e)$ to calculate the intensity of the GPI line radiation from the computed fluctuations in the turbulent density and temperature. This simulated light intensity pattern is then analyzed and directly compared with the NSTX GPI intensity data.

The results described in this paper model NSTX shot #112825 (the same shot discussed in [9]), which was an L-mode discharge and used He gas puffing to simplify the calculation of $n_0(x)$. It should be noted that techniques have been developed to calculate $n_0(x)$ for deuterium using the neutral particle code DEGAS 2 [8], and recently a new fitting formula was obtained for the neutral gas profiles in NSTX shots with D gas puffing. There is a large and ever-growing database of GPI movies on NSTX using D gas puffing which can be analyzed by the techniques described here.

For the shot analyzed here, several points of agreement have been found between the turbulence simulations and GPI data, and key parameters have been identified. Our goal is to choose parameters such that the simulated turbulence satisfies the following properties: (i) the turbulence is intermittent and blobs are emitted in random bursts, similar to what is seen in the NSTX GPI "movie" for this shot (*FIG. 4*), (ii) the radial profile of the GPI radiation intensity $I(\Delta r)$ computed with the SOLT synthetic diagnostic agrees reasonably well with the data (*FIG. 5*), and (iii) the radial skewness profiles, $S(\Delta r)$, for the density, temperature and GPI intensity are similar to those inferred from the data in the radial region where the fluctuations are large, viz. away from the blob birth zone ($\Delta r > 0$). Moreover, we want to demonstrate quantitatively that the turbulence predicted by the SOLT code generates blobs with properties similar to those observed in the GPI movies for NSTX. Thus, we have used a blob tracking algorithm to compile a database of blobs, and we computed the blob statistics for both the simulation and the NSTX data, comparing (iv) the PDF of blob size a_b (*FIG. 6*) and (v) the PDF of blob velocity v_x.

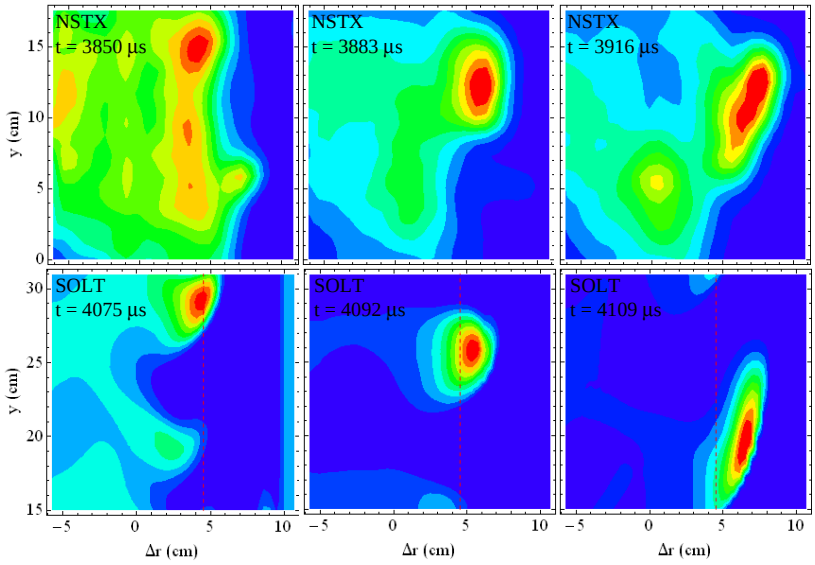

FIG. 4 GPI emission pattern ($\delta I / I$) in the Δr-y plane for three equally-spaced frames taken from the NSTX GPI data (top row) and the SOLT simulation with synthetic GPI diagnostic (bottom row).

In *FIG. 4*, we show three equally-spaced snapshots in time of the GPI intensity pattern $\delta I / \langle \bar{I} \rangle$, where $I(\Delta r, y, t)$ is the GPI

intensity mapped to the midplane, $\delta I = I - \langle \bar{I} \rangle$, and again an overbar denotes a zonal average and <…> denotes a time average. The top row in *FIG. 4* is taken from the NSTX GPI "movie" (time-sequence of frames) for shot #112825, and the bottom row is taken from the SOLT simulation with synthetic GPI diagnostic. From watching the entire sequence of frames, one sees that the simulation intermittently produces blobs as in the experiment. The simulated blob shown in *FIG. 4* has roughly the same shape and radial velocity (within a factor of 2) as in the NSTX data, and it develops a similar elongation in the direction of the flow. We also see that v_x matches better than v_y. This is expected because the 2D simulation does not have all of the physics needed to compute the radial E field (and thus v_y); however, it can describe the blob charge polarization physics responsible for v_x. A more quantitative analysis of v_x can be obtained from blob tracking, as discussed subsequently. We note that agreement in the intensity I itself is poorer due to the far SOL discrepancy discussed in connection with *FIG. 5*.

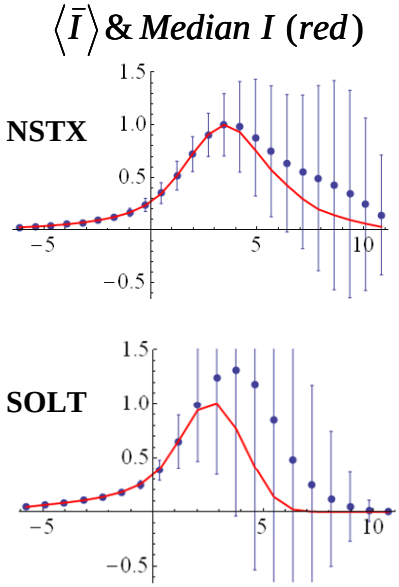

FIG. 5 Radial profile of GPI intensity, I(Δr) for both the NSTX data and the SOLT simulation.

In *FIG. 5*, the radial profiles of the GPI intensity I(Δr) are compared for both the data and the simulation. In each case, the red curve gives the *median* value in time of the y-averaged intensity at each radius. The blue dots indicate the *mean* (y- and t-averaged) value of I; the blue bars give the standard deviation with respect to the mean. Both the experimental and code data were processed in the same way, and the peak intensity was normalized to 1.0 in each case. Note that the simulated intensity in the SOLT code peaks at the correct radial position, just inside the radial position of the sheath at Δr = 4.5 cm. The simulated intensity is much smaller than the measured value for Δr > 5 cm, which indicates that the value of the sheath conductivity was too large in this run (cooling the far SOL too much). Thus, further optimization of parameters is possible in the simulation.

We do not show here the radial profiles of the skewness S of the GPI intensity, but give the following comments about the comparison. The simulation reproduces the general shape of S(Δr) in the experimental data: the skewness is negative in the core, goes through zero near the LCS, and rises monotonically to large values at the wall). However, matching the intensity data in the region near the LCS where S is small requires some care due to the non-monotonic dependence of the radiation function on T_e. One must adjust the core heat source and the dissipation parameters so that the mean turbulent temperature profile does not greatly exceed the measured profile in that region. Thus, the skewness near the separatrix can be used as a diagnostic for the dissipation parameters.

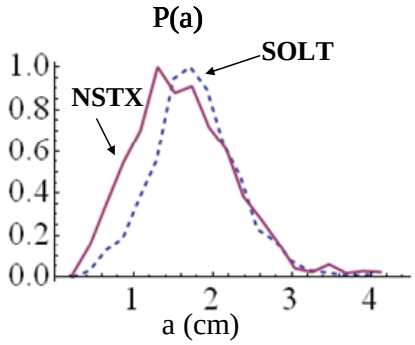

FIG. 6 PDF of the blob size a in NSTX data and SOLT simulation

In *FIG. 6* we show the probability distribution function (PDF) of the (poloidal) blob half-width *a*. To get these curves, a database of blobs was created by defining a selection criterion for blobs and applying it to the turbulence data over the the spatial range 0 < Δr < 10 cm and covering a

time slice of 1200 μs. Both the experimental and simulation data were processed in the same way. We find that the results from both the SOLT simulation and the NSTX data analysis give a most probable blob size in the range a ~ 1.5 – 2.0 cm, and the width of the PDF also agrees fairly well. It should be pointed out that the shape of the PDF is sensitive to the criteria used in constructing the blob database, the types of filtering and data smoothing, etc. For example, the results in *FIG. 6* used no poloidal smoothing; when significant smoothing in y was used, the most probable blob size increased to a = 2.5 cm.

Blob theory [1] makes a prediction for the most stable (and therefore most probable) blob size in the sheath-connected regime: $a = a_* \equiv \rho_s (L_\parallel^2 / \rho_s R_c)^{1/5}$, where R_c is the radius of curvature of the B field.. For the parameters of the simulation discussed in this section, a_* = 2.3 cm. Although all of the blobs in the simulation are not in this parameter regime, we would expect a_* to be a typical scale size for the blobs, and *FIG. 6* shows that this is true to within a factor of 2.

The PDF $P(v_x)$ of the blob radial velocity (not shown) agrees to within a factor of 2 between the simulation and the experiment. For this NSTX shot, the peak of the distribution is at v_x = 0.5 km/s, whereas for the simulation the peak is at v_x = 0.8 km/s and the latter distribution has a long tail at high v_x that is not present in the NSTX data. The reason for this factor of 2 discrepancy is under investigation using optical flow techniques in collaboration with T. Munsat. Again the simulation PDF is broader than the experimental one. Both the larger v_x and broader distribution in the simulation are consistent with the plasma in the blob birth zone being too far away from marginal stability (turbulence too strong), which is consistent with other aspects of the analysis. This suggests that the dissipation near the LCS in the simulation is too weak. Finally, we point out that the values of blob velocity obtained from this analysis falls within the limits predicted by blob theory [9].

We have found that the five properties listed above are sensitive to the parameters of the simulation model, and we have tried to constrain these parameters by experimental data for the given shot. In the NSTX modeling runs, we set the flow damping parameter to zero, $\nu_{py} = 0$ (see Sec. 4), to obtain the full sheared-flow dynamics and coherent structures that were blob-like (not radial streamers). The restoration term $\propto \nu_T$ in the electron temperature equation was used to damp the turbulent fluctuations near the separatrix and to restore the turbulent T profile to the specified source profile (which was based on Thomson scattering measurements). For these comparisons, both the time- and y-averaged density and temperature profiles were constrained to match experimental data. Optimizing ν_T gave more intermittent behavior and a better match on the skewness profile $S_I(x)$ of the GPI intensity.

In addition to damping parameters, it was important to optimize the sheath location. To explain this, we note that there are three radial regions with different topologies in the simulation: (1) the edge region inside the LCS ($\Delta r < 0$) in which field lines are closed, (2) the near-SOL region just outside the separatrix ($0 < \Delta r < \Delta r_{sh}$) in which the parallel connection to the sheaths is assumed weak ($L_\parallel \to \infty$) due to X-point effects, and the far-SOL region ($\Delta r > \Delta r_{sh}$) with a finite $L_\parallel$, resulting in sheath effects playing a prominent role ("sheath-connected"). The sheath conductivity in the simulation vanishes in the edge region and increases sharply in the SOL (tanh profile); we refer to the inflection point of the curve as Δr_{sh} and the width of the transition as L_{sh}. The GPI intensity profile $I(\Delta r)$ was found to be sensitive to the position of the sheath entrance (Δr_{sh}). For the optimal sheath location, the degree of intermittency was sensitive to the parameter L_{sh} (width of the tanh function), which controlled the sheath penetration into the region just outside the separatrix. For L_{sh} too large, the turbulence was damped; for L_{sh} too small, the turbulence activity was too high (too many blobs, not intermittent), but for intermediate L_{sh} the code obtained a sustainable turbulent state that was highly intermittent, as observed in the NSTX GPI movies.

In conclusion, when the input parameters are properly optimized to give the correct physical regime, the 2D SOLT simulations can reproduce many generic features of boundary turbulence seen in NSTX. Features reproduced qualitatively by the simulations include statistical quantities (skewed PDFs, power law frequency spectra, correlation lengths, and skewness vs. radius) and qualitative features seen in the GPI and probe data (such as spatial and temporal intermittency, blob generation, interaction between sheared flows and edge turbulence, etc.). Our analysis is similar to previous comparisons of ESEL code simulations with TCV edge turbulence data [10], with the added advantage here that the experimental and simulated GPI data provide the full 2D structure of the turbulence. This allows direct evaluation of both components of blob velocity and the poloidal blob size. We have found that quantitative agreement for a given shot is sensitive to the radial width of the transition region (from separatrix to sheath-connected field lines) and to the degree of dissipation in the model. For the shot analyzed here (#112825), the best-fit simulations have a sheath region extending close to the separatrix, with the result that the blobs are best characterized as transitioning from the disconnected to the sheath-connected regimes of blob theory as they propagate radially outward.

6. Summary

Intermittent turbulent transport is an important issue for ITER, impacting design parameters such as the efficiency of the divertor, the lifetime of the first wall, and the heating efficiency of ICRF antennas. Although much is known about the scaling of the radial velocity of turbulent objects such as blobs and ELMs, we still do not know how their production (source rate) scales with physical parameters, and thus we cannot predict the turbulent flux or its statistics without numerical simulations. Simulations show that there is a subtle interplay between edge turbulence, sheared flows, and dissipation (plasma and sheath). This interplay controls the intermittent transport of particles, energy and momentum. The agreement obtained recently between our 2D simulations with 2D imaging data in NSTX is encouraging and should lead to further progress in understanding the physics of turbulence saturation and blob generation.

*This research was supported by the US DOE under grants DE-FG02-97ER54392 and DE-FG02-02ER54678.

[1] KRASHENINNIKOV, S.I., D'IPPOLITO, D.A., and MYRA, J.R., J. Plasma Phys. **74** (2008), doi: 10.1017/S0022377807006940.
[2] COPPI, B., Nucl. Fusion **42**, 1 (2002); Coppi, B., et al., in *Proceedings of the 2006 European Physical Society International Conference on Plasma Physics* (European Physical Society, Rome, 2006) Paper P4.017.
[3] MYRA, J.R, et al., in *Plasma Physics and Controlled Nuclear Fusion Research 2006* (IAEA, Vienna, 2007), paper IAEA-CN-149-TH/P6-21.
[4] DIAMOND, P. H., McDEVITT, C. J., and GURCAN, Ö. D., HAHM, T. S., and NAULIN, V., Phys. Plasmas 15, 012303 (2008), and references therein.
[5] RUSSELL, D.A., MYRA, J.R, and D'IPPOLITO, D.A., Phys. Plasmas **14**, 102307 (2007).
[6] MYRA, J.R., and D'IPPOLITO, D.A., Phys. Plasmas **12**, 092511 (2005).
[7] MYRA, J.R, RUSSELL, D.A., and D'IPPOLITO, D.A., Phys. Plasmas **15**, 032304 (2008).
[8] STOTLER, D.P., BOEDO, J., LEBLANC, B.P., MAQUEDA, R.J., and ZWEBEN, S.J., J. Nucl. Mater. **363-365**, 686 (2007).
[9] MYRA, J.R., D'IPPOLITO, D.A., STOTLER, D.P. , ZWEBEN, S.J., LEBLANC, B.P., MENARD, J.E., MAQUEDA, R.J., BOEDO, J., Phys. Plasmas **13**, 092509 (2006).
[10] GARCIA, O.E., HORACEK, J., PITTS, R.A., NIELSEN, A.H., FUNDAMENSKI, W., NAULIN, V. and JUUL RASMUSSEN, J., Nucl. Fusion **47**, 667 (2007).